Graph Neural Networks with Directional Encodings for Anisotropic Elasticity

Anonymous authors
Paper under double-blind review

Abstract

Simulating the behavior of nonlinear and anisotropic materials is a central problem with applications across engineering, computer graphics, robotics, and beyond. While conventional mesh-based simulations provide accurate and reliable predictions, their computational overhead typically prevents their use in interactive applications. Graph neural networks (GNN) have recently emerged as a compelling alternative to conventional simulations for time-critical applications. However, existing GNN-based methods cannot distinguish between deformations in different directions and are thus limited to isotropic materials. To address this limitation, we propose a novel and easy-to-implement GNN architecture based on directional encodings of edge features. By preserving directional information during message passing, our method has access to the full state of deformation and can thus model anisotropic materials. We demonstrate through a set of qualitative and quantitative evaluations that our approach outperforms existing mesh-based GNN approaches for modeling anisotropic materials.

1 Introduction

From plant leaves to animal muscle and from woven textiles to fiber-reinforced composites—many natural and engineered materials are strongly anisotropic, *i.e.*, their stress response varies significantly depending on the direction of deformation. Simulating such anisotropic materials properties is crucial for many applications in science and engineering (1). Conventional simulation methods typically rely on mesh-based finite element discretizations for numerical solutions of the underlying partial differential equations. While these methods can capture intricate material behavior with high accuracy, they come at a substantial computational cost. Striking a balance between accuracy and efficiency, learning-based methods have emerged as a promising alternative to conventional simulations. Arguably the closest analogy to mesh-based simulation is a mesh-based deep neural representation. Indeed, existing works built on mesh-based graph neural networks (MGNN) have shown promising results (2; 3). While existing MGNN methods have focused on isotropic materials so far, accounting for anisotropy might seem a straightforward extension. Unfortunately, the message passing architectures of current MGNNs rely on spatial averaging of edge features, which discards all directional information on deformation. As we show in our analysis, discarding directional information means that existing MGNNs are unable to model anisotropic materials.

In this work, we present a novel feature encoding scheme designed to preserve directional information during message passing. We decompose edge features into components along three material-space basis vectors and aggregate these components separately during message passing. In this way, feature averaging takes into account the material-space orientation of the edges, leading to significantly improved preservation of anisotropic information. This improvement requires minimal changes to standard mesh-based graph neural networks, thus allowing for easy integration into existing frameworks. We validate our approach on a set of qualitative and quantitative examples and demonstrate that our approach outperforms the state-of-the-art method for capturing material anisotropy.

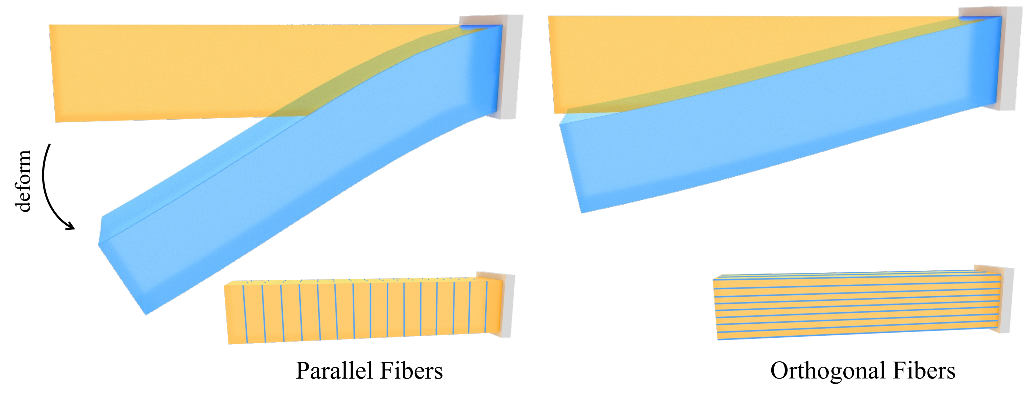

Figure 1: Anisotropic Elasticity. We apply our approach to model the nonlinear deformation of an elastic cantilever beam under gravitational load. The beam is made from an isotropic base material augmented with reinforcing fibers (see insets). On the left, fibers are oriented in parallel to the direction of gravity, which leads to only minor stiffening compared to the base material. On the right, fibers run along the axis of the beam, leading to significantly reduced deflection for this load case. Rest and deformed states are shown in orange and blue, respectively.

2 Related Work

Simulation of Deformable Objects Simulating deformable objects plays a pivotal role across various disciplines, including mechanical engineering, computer graphics, and robotics. Among existing approaches, which include particle-based (4; 5; 6), grid-based (7; 8; 9; 10) and hybrid methods (11; 12), mesh-based representations are arguably the most prevalent choice (13; 14; 15; 16). The computer graphics community has made great strides in efficient, robust, and accurate mesh-based simulation of deformable bodies (17; 18; 19; 20; 21). Although dimension reduction techniques exist (22; 23; 24; 25), the associated computational costs for native scale simulation are often too significant for real-time applications or rapid design explorations. Our approach falls into the same category of using mesh representation for the input geometry, however, we use mesh-based graph neural networks to reduce online computation time significantly.

Simulation of Anisotropic Materials Realistic simulating of many phenomena in nature must take into account their inherent material anisotropy, *e.g.* muscle deformation (26), plant biomechanics (27), material fracture (28), *etc*. Within the scope of this work, we focus on simulating deformable objects within the hyperelastic regime. Within this realm of research, many forms of anisotropic energies have been extensively studied, for instance, transverse isotropic elasticity (29; 30; 31), orthotropic elasticity (32), and generalized anisotropic elasticity (33; 34). We focus on transverse isotropic elastic material where a base isotropic material is augmented with freely oriented fibers to achieve directional-dependent properties. This allows for easy integration into existing isotropic formulations. While anisotropic material properties have been extensively studied for mesh-based simulation, representing directional-dependent behavior with neural representation remains unexplored. We identify a key limitation factor for existing mesh-based neural representations and propose a simple yet effective strategy for better capturing material anisotropy.

Neural Representation Deep neural representations hold substantial promise as alternatives for modeling complex physical systems while significantly reducing computational requirements when compared to conventional approaches (35; 36; 37). One stream of research relies on ground-truth simulation data for learning surrogate models, *e.g.* for fluid dynamics (38), character animation (39), and modeling nonlinear material properties (40; 41). With the advancement of physics-informed learning (42), another line of research leverages physical laws directly as loss functions to enable self-supervised learning (43; 44; 45; 46). In this manner, neural networks learn not only from existing data but also from the inherent physics governing the system. We also opt for an unsupervised training strategy where the variational formulation of the physics laws directly as loss functions.

However, to the best of our knowledge, our work is the first to explore material anisotropy for neural representations of deformable solids with graph neural networks.

Mesh-based Graph Neural Networks Recent advancements in graph-based neural network architectures (47; 48; 49) offer a new paradigm for soft-body simulations (2; 50; 51). Specifically, mesh graph networks have emerged as a promising alternative to conventional finite element methods for simulating, for instance, fluid (52; 53), solid (54; 55; 2), cloth (3), *etc*. Unlike grid-based methods (56; 57; 35), their unstructured nature allows for easy generation of simulation domains and resolutions. Most related to our approach is MeshGraphNet (2), where an encoder-processor-decoder network architecture is leveraged to predict accelerations per time step. While their approach is able to capture a range of phenomena governed by physics PDEs, challenges remain for material anisotropy. We propose a novel and easy-to-implement edge feature decomposition operation to encode directional information during training. As we demonstrate in the result section, this modification significantly improves the performance of learning anisotropic material properties.

3 Method

In this section, we describe the machinery required for training GNNs with directional encodings. Our approach builds upon an encoder-processor-decoder network architecture with a novel edge feature decomposition scheme aimed at capturing material anisotropy (Sec. 3.1). We adopt a self-supervised training paradigm and use the variational formulation for implicit Euler as the loss function 3.2. We provide sampling, training, and implementation details in Sec 3.3.

3.1 Model Architecture

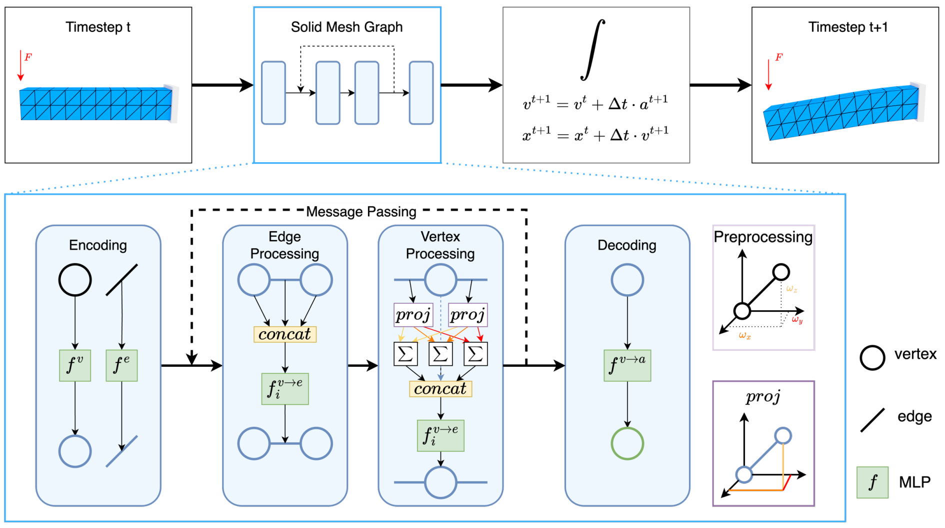

Figure 2: Pipeline. Our method takes the current states of a deformable object and its boundary conditions as input and predicts end-of-time-step accelerations using a graph neural network. These accelerations are then used to obtain the deformed state for the next time step (first row). We leverage an encoder-processor-decoder architecture and propose a novel edge decomposition operation to encode directional information during message passing (second row).

We define the simulation mesh as a graph $G = (\mathbf{V}, \mathbf{E})$ with nodes $\mathbf{V}$ and edges $\mathbf{E}$. Each node is associated with a coordinate vector $\mathbf{x}$ and additional physical parameters such as mass, external forces, and Dirichlet boundary conditions. We refer to these parameters as vertex features $\mathbf{v}$. Likewise, we use $\mathbf{e}$ to denote edge features, which include relative vertex positions and fiber orientations.

Our neural representation builds on the encode-process-decode architecture (48), where two distinct multilayer perceptrons (MLPs) are used as encoders to extract vertex and edge features. The encoded features are then processed with a set of MLPs during a fixed number L of message passing steps. In each step, all edge and vertex features are processed using the same MLPs, but each step has its own vertex and edge MLP. Finally, a decoder MLP is used to transform vertex features to end-of-time-step accelerations. The predicted accelerations are used to update vertex positions. See Figure 2 for an overview.

Encoding and Decoding Our encoder and decoder MLPs largely follow MeshGraphNets (2). The input vertex and edge features are transformed into latent feature vectors through encoder MLPs f_v and f_e,

$$\tilde{\mathbf{v}} = f_v(\mathbf{v}), \quad \tilde{\mathbf{e}} = f_e(\mathbf{e}), \tag{1}$$

where $\tilde{\mathbf{v}}$ and $\tilde{\mathbf{e}}$ denote updated feature vectors. The vertex decoder $f_{v \to a}$ maps vertex features to end-of-time-step accelerations for a given vertex,

$$\mathbf{a} = f_{v \to a}(\mathbf{v}) \ , \tag{2}$$

which are then used to compute end-of-step positions.

Direction-aware Message Passing Our key contribution lies in the message passing step where we leverage directional encodings to better preserve information on anisotropic states of deformation. Specifically, we update per vertex and edge feature as

$$\begin{aligned} \tilde{\mathbf{e}} &= \mathbf{e} + f_{v \to e}(\mathbf{e}, \mathbf{v}_0, \mathbf{v}_1), \\ \tilde{\mathbf{v}} &= \mathbf{v} + f_{e \to v}(\mathbf{v}, \sum_{\mathbf{e}_j \in \mathcal{N}_i} \omega_{x,j}\mathbf{e}_j, \sum_{\mathbf{e}_j \in \mathcal{N}_i} \omega_{y,j}\mathbf{e}_j, \sum_{\mathbf{e}_j \in \mathcal{N}_i} \omega_{z,j}\mathbf{e}_j), \end{aligned} \tag{3}$$

where $\mathbf{v}_0$ and $\mathbf{v}_1$ are the vertex features for the two endpoints of a given edge, $\mathbf{e}_j$ loops over the features for all edges incident to vertex i, and $f_{v \to e}$ and $f_{e \to v}$ are the edge and vertex processor MLPs respectively. We use $+$ to denote residual connections (58).

It is important to note that MeshGraphNet (2) aggregates edge features directly to update vertex features. This operation, however, does not distinguish deformations in different directions. To understand this problem, consider a mesh edge that is oriented along the x-axis in material space. Since the edge stores relative position between its endpoints, it cannot sense deformation along the y- and z-directions, which leave relative positions along the x-axis unchanged. Nevertheless, the feature aggregation scheme used in MeshGraphNets does not consider this dependence of sensing capacity on edge orientation, which ultimately limits its ability to capture directional deformation and model material anisotropy. By contrast, our novel encoding scheme projects mesh edges onto an orthonormal material-space basis such as to measure their capacity to sense deformation along different coordinate axes. The resulting coordinates are then used to decompose the original edge feature into three weighted components that are averaged individually. Using this directional encoding, an edge that aligns well with a given direction of deformation is given more authority to determine the averaged feature than an edge that is almost orthogonal to that direction. As a result, our method is able to preserve directional deformation during message passing and can thus better model anisotropic materials. We note that the edge weights $\omega_{x,j}$, $\omega_{y,j}$, and $\omega_{z,j}$ are computed from the rest state edge vectors and remain constant during training. Concretely, the weights for a given edge $\mathbf{E}_j$ are computed as

$$\omega_{x,j} = \frac{\mathbf{E}_j}{||\mathbf{E}_j||} \cdot \mathbb{E}_x, \quad \omega_{y,j} = \frac{\mathbf{E}_j}{||\mathbf{E}_j||} \cdot \mathbb{E}_y, \quad \omega_{z,j} = \frac{\mathbf{E}_j}{||\mathbf{E}_j||} \cdot \mathbb{E}_z, \tag{4}$$

where $\mathbb{E}_x$, $\mathbb{E}_y$ and $\mathbb{E}_z$ are unit-length basis vectors. We further note that this modification requires minimal changes to standard mesh-based graph neural network architectures, allowing for easy integration of our approach into an existing framework. As we demonstrate in the result section, our directional feature encoding scheme leads to significantly improved performance for learning material anisotropy.

3.2 PHYSICS-BASED LOSS FUNCTION

Spatial Discretization We resort to tetrahedral finite elements with linear basis functions to model the nonlinear dynamics of deformable solids. Our network operates on the edges and nodes of the simulation mesh and performs message passing on the corresponding graph. Adhering to standard finite element practice, our loss functions by summation of per-element potentials.

Loss Function To allow for efficient self-supervised learning, we formulate our loss function to directly penalize the violation of the dynamic equilibrium conditions. To enable robust time stepping for larger step sizes, we use backward Euler integration, *i.e.*, a first-order accurate implicit time stepping scheme (59). Instead of directly solving the resulting system of nonlinear equations, we follow the variational formulation of Martin *et al.* (17) and convert the root finding problem into an energy minimization problem. We use the corresponding incremental potential as our physics-based loss function during training. Defining end-of-time-step positions and accelerations as $\mathbf{x}^{t+1}$ and $\mathbf{a}^{t+1}$, our total loss function reads

$$\mathcal{L}_{\text{total}}(\mathbf{a}^{t+1}, \mathbf{x}^{t+1}) = \mathcal{L}_{\text{elastic}}(\mathbf{x}^{t+1}) + \mathcal{L}_{\text{external}}(\mathbf{x}^{t+1}) + \mathcal{L}_{\text{kinetic}}(\mathbf{a}^{t+1})\ . \tag{5}$$

Our $\mathcal{L}_{\text{elastic}}$ term captures the elastic energies for both isotropic and anisotropic deformation. We focus on transversely isotropic materials, where anisotropic fibers are embedded in an isotropic base material. Such materials are widely used for physics-based modeling of, *e.g.*, fiber-reinforced composites, and biological tissue. We adopt the widely used Saint Venant–Kirchhoff model (60) for the isotropic base material and augment it with an anisotropic term that models the effect of embedded fibers with a given orientation. The elastic energy for a given tetrahedron element is defined as

$$\mathcal{L}_{\text{elastic}}(\mathbf{x}^{t+1}) = \bar{v}\left(\frac{\lambda}{2}(tr(\mathbf{E}))^2 + \mu tr(\mathbf{E}^2) + \kappa(\mathbf{d}^{\mathsf{T}}\mathbf{F}^{\mathsf{T}}\mathbf{F}\mathbf{d} - 1)^2\right)\ , \tag{6}$$

where $\mathbf{E} = \frac{1}{2}(\mathbf{F}^{\mathsf{T}}\mathbf{F} - \mathbf{I})$ is the nonlinear Green strain, $\mathbf{F}$ is the deformation gradient, and $\mathbf{d}$ is the fiber direction. Furthermore, $\bar{v}$ is the undeformed volume of an element, and λ and μ are Lamé parameters for defining the material properties. Finally, κ is the Young's modulus for fiber stiffness.

The kinetic energy term is defined as

$$\mathcal{L}_{\text{kinetic}}(\mathbf{a}^{t+1}) = \frac{1}{2}(\Delta\mathbf{v}^{t+1})^{\mathsf{T}}(\Delta\mathbf{v}^{t+1} \odot \mathbf{m}_v), \tag{7}$$

where Δt is the simulation time step size, $\Delta\mathbf{v}^{t+1} = \Delta t\mathbf{a}^{t+1}$ are velocity increments and $\odot$ denotes element-wise vector-vector multiplication between the velocity increments and masses for all vertices within an element.

We further define the external energy corresponding to the work done by external loads as

$$\mathcal{L}_{\text{external}}(\mathbf{x}^{t+1}) = \mathbf{f}_{\text{ext}} \cdot \mathbf{x}^{t+1}, \tag{8}$$

where $\mathbf{f}_{\text{ext}}$ is a vector containing all external forces.

3.3 Training and Implementation Details

Sample Generation We generate our training samples using combinations of simple geometries, *e.g.* rectangular and cylindrical beams (36 in total) with different mesh topologies and resolutions. The training mesh resolution is between 60 to 120 elements. We uniformly sample the force direction and magnitude ($0 - 10kN/m^3$) applied to each mesh element. For non-uniform loading scenarios, we add additional forces to each element with a probability of 5%. Magnitude and direction are randomly sampled for each element ($0 - 15kN/m^3$). Finally, we include traction samples with a probability of 10% with fixed direction in $+z$ axis and amplitudes between $0 - 100kN/m^3$. For material anisotropy, we uniformly sample fiber orientations and magnitudes between $0 - 10E$ where E is the Young's Modulus of the base material which is fixed to be $100kPa$. To increase stability for long-time inference rollouts, we find it crucial to sample not only undeformed states with random forces but also deformed states with non-zero kinetic and elastic energies. We apply the above parameter sampling procedure to these pre-deformed samples as well.

Training Our framework is implemented in C++ using LibTorch. We use the Adam (61) optimizer with a learning rate of 5×10^{-5} and a weight decay rate of 10^{-4} per one hundred iterations. Each training sample is unique and randomly sampled. The batch size is set to 1 and we train a total of $672,000$ epochs. All of our MLPs have two hidden layers with 128 neurons per layer and SiLU activation functions (62). Layer normalization is applied to all layers except the final decoder MLP. All input features except the one-hot encoded anchored vertices are normalized. The encoder MLPs produce output features of size 128, while the vertex decoder yields features of size 3. Following MeshGraphNets, we perform 15 message-passing steps.

Vertex input features consist of a one-hot-ended vector containing Dirichlet boundary conditions, vertex velocities, vertex mass and vertex external forces. Edge input features consist of two vectors containing the edge direction of both undeformed configuration and current deformation. Both vectors are normalized and their norm is added as a separate feature. Additionally, all edges contain another vector with fiber direction and magnitude.

During training, we introduce perturbations to both nodal velocity and positions using zero-mean noise. The variance for velocities is stochastically sampled from the range of $0-5\times10^{-2}m/s$, while the variance for position noise falls within the interval of $0-10^{-3}m$. This perturbation process, akin to MeshGraphNets, plays a pivotal role in ensuring the stability of the neural network for long rollouts. The network is trained on a workstation with an *AMD Ryzen 7 5800X* CPU and an *NVIDIA GeForce RTX 3080Ti* GPU. Training takes around 5 days, whereas inference takes $9ms$ for a mesh of 100 elements.

The Lamé parameters are computed from Young's modulus (100kPa) and Poisson's ratio (0.48) of a soft rubber-like material. When performing time stepping, we use a step size Δt of $0.02s$. We will release our code upon acceptance.

4 RESULTS

In this section, we compare our results to the state-of-the-art mesh graph neural network, MeshGraphNets (2) on a set of qualitative and quantitative experiments. Since MeshGraphNets are trained in a supervised fashion, for fair comparisons, we implemented an unsupervised version using their network architectures with only modifications to the loss function to accommodate self-supervised learning. We demonstrate that our approach outperforms this baseline in terms of convergence speed, the ability to capture material anisotropy, and volume preservation for nearly incompressible materials. We further use a standard finite element solver to generate ground truth data for reference.

Convergence We begin by comparing our approach with MeshGraphNets for different numbers of test rollouts (Figure 3). We generate 15 random configurations, *i.e*. different mesh topologies, force magnitudes, and directions, as test sets for all approaches and compute the difference in energy with respect to the ground truth value obtained from our reference simulation. After each training iteration, we evaluate all networks on the same test sets for different numbers of rollout steps in order to gauge their stability for sequences of different lengths. In particular, longer rollouts are useful to test whether predictions are converging toward static equilibrium. As can be seen from Figure 3, our approach consistently improves on MeshGraphNets, showing substantially faster convergence in all cases. It can also be noted that our method converges to equilibrium states with lower total energy.

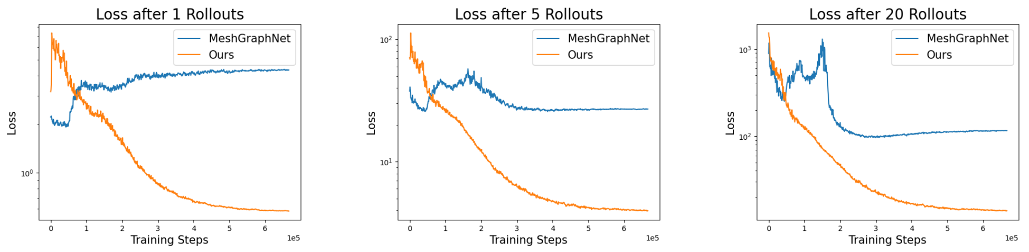

Figure 3: Network convergence. We compare the convergence behavior for our approach with MeshGraphNets on a test set for different rollout lengths. As can be seen in these figures, our approach converges to lower energy states much faster while remaining stable for longer horizons.

We attribute the significant discrepancy of MeshGraphNets to its limited ability to capture the anisotropic fibers. To verify this hypothesis, we visualize the energy difference to ground truth data for the fiber term and the sum of all terms separately. In this example (Figure 4), a beam with fibers along its long axis is loaded along the fiber direction. As can be seen from the plot shown to the left, the error in the fiber term for MeshGraphNets dominates the overall energy profile, leading to 10 times larger error compared to our method.

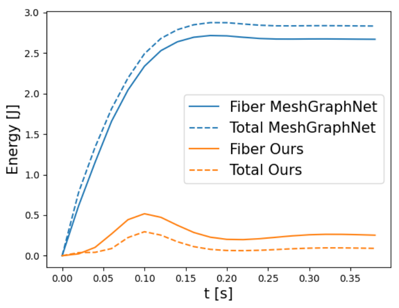

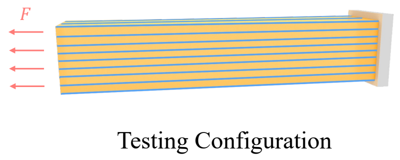

Figure 4: Fiber and total energy error. A beam under uni-axial tension with fibers aligned with the direction of loading (*right*). We report the fiber and total energy error compared to simulation references (*left*). Due to the limited capability of capturing material anisotropy, the error from the fiber term dominates the overall error leading to significant deviation from ground truth data. Our approach, on the other hand, demonstrates 10 times higher accuracy.

Anisotropic Elasticity To quantify the difference in terms of capturing anisotropic elasticity, we compare our approach with MeshGraphNet on a set of uniaxial loading test cases with fiber reinforcements in different magnitudes and directions (see Figure 5). When fiber reinforcements are collinear with the loading direction, they introduce strong resistant forces upon tensioning. Consequently, larger stress magnitudes for a given strain rate. As can be seen in the slopes of the curves in Figure 5 (a,b), our model successfully captures this highly anisotropic behavior for different fiber stiffness whereas MeshGraphNets leads to poor matching behavior. Note that for strong fibers, the predictions from MeshGraphNets deviate already for small strain. When fibers are aligned orthogonal to the loading directions, they have minimal effects on the directional stress magnitude. This behavior is again captured by our model (Figure 5 (c)).

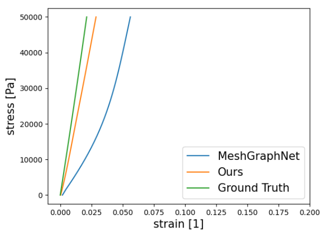

(a) Strong fibers ($\kappa = 5E$) in parallel direction

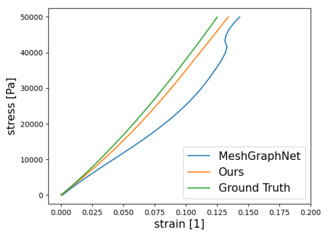

(b) Weak fibers ($\kappa = E/5$) in parallel direction

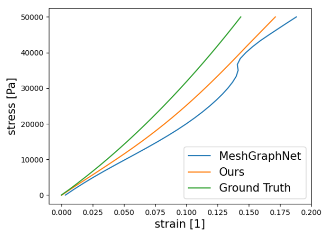

(c) Fibers ($\kappa = E/5$) in orthogonal direction

Figure 5: Strain-stress curves. We compare our approach with MeshGraphNets on a set of uniaxial loading cases with different fiber orientations and magnitudes. We use E to denote Young's modulus of the base material. The predictions from our approach track the ground truth solution consistently better than MeshGraphNets and do not suffer from instabilities for larger strain rates.

Volume Preservation In addition to capturing explicit material anisotropy, direction encodings also facilitate learning volumetric effects pertaining to the Poisson ratio, *i.e.* when a tension load is applied in one direction, causing the orthogonal directions to contract in order to preserve the material volume. In this experiment, we compare our approach and MeshGraphNets to the reference simulation on volume preservation of a beam under a constant tensile force. We report the maximum relative percentage error over all elements in Figure 6. As can be seen from this plot, MeshGraphNets leads to volume change up to 60% whereas our approach exhibits almost zero volume changes.

Tip Displacements Complementing previous examples where tension modes are examined, we now shift to bending modes for more analysis. In this example, we quantitatively validate our approach by comparing the tip displacement error for a cantilever beam to its reference simulation.

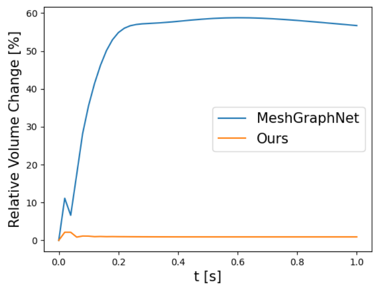

Figure 6: Volume preservation error. We plot the maximum relative percentage error for all elements in a deformed beam under tension. While our directional feature encoding leads to almost zero volume change compared to the simulation baseline, MeshGraphNets permits volume changes up to 60%.

We consider two extreme testing scenarios for fiber orientations, one that is aligned with gravity in its rest shape (more deformation) and one that is orthogonal to it (less deformation). They are referred to as *parallel* and *orthogonal* in Table 1. We test all approaches with two beam topologies, namely rectangular (row *1-6*) and cylindrical beams (row *7-12*). For this set of experiments, we use the same stiffness for both the base material and the fibers. As reported in Table 1, our approach consistently outperforms the baseline method in terms of accuracy across all tested scenarios and beam topologies.

Fiber Orientation	Beam Topology	Method	Tip Displacement Error(m)
parallel	rectangular	MeshGraphNets	0.0399
parallel	rectangular	**ours**	**0.0119**
orthogonal	rectangular	MeshGraphNets	0.0902
orthogonal	rectangular	ours	**0.0510**
parallel	cylindrical	MeshGraphNets	0.1111
parallel	cylindrical	**ours**	**0.0776**
orthogonal	cylindrical	MeshGraphNets	0.1400
orthogonal	cylindrical	**ours**	**0.0977**

Table 1: Tip displacement comparisons. We consider two types of beam structures under gravitational force with one end of the beams fixed and leaving the other end free. Reinforcement fibers are set to be either parallel or orthogonal to gravity. As can be seen from the tip displacement errors reported, our approach demonstrates significantly higher accuracy compared to MeshGraphNets.

Imbalanced Forces In this experiment, we consider the physically imbalanced force in the configuration generated by MeshGraphNets and our approach. The gradient of our loss function w.r.t. nodal positions amounts to the force equilibrium condition governed by Newton's second law of motion, which should vanish at stable configurations. We therefore refer to the nonzero gradients as imbalanced forces. In Table 2, we report the imbalanced force magnitude from network predictions for a cantilever beam under static force equilibrium configurations. Same as in the previous example, we use the same stiffness for both the base material and fiber reinforcements. We apply a force density with its direction with gravity with two magnitudes ($1000N/m^3$ and $5000N/m^3$). The fiber directions are varied from 45 to 90 degrees with 90 being orthogonal to the force direction. As can be seen from the statistics for average and maximum nodal imbalance forces, our approach reduces the mean error by 80% on average and the maximum error up to 90%.

Generalization Finally, we demonstrate that our network generalizes to unseen geometries with different fiber layouts (Figure 7). In the first example, we add fibers to a T-shaped deformable object to resist bending load whereas in the second one, the fibers resist compression force for a Y-shape geometry. The applied forces and fiber orientations are shown in the insets.

Fiber Direction	Force Density (N/m^3)	Method	Imbalanced Force (N) Max/Mean
45°	5000	MeshGraphNets	77.84 / 16.71
45°	5000	**ours**	**14.01 / 3.747**
45°	1000	MeshGraphNets	46.40 / 12.20
45°	1000	**ours**	**4.321 / 1.446**
60°	5000	MeshGraphNets	76.36 / 16.83
60°	5000	**ours**	**18.92 / 4.205**
60°	1000	MeshGraphNets	42.98 / 12.07
60°	1000	**ours**	**4.760 / 1.608**
90°	5000	MeshGraphNets	67.89 / 16.25
90°	5000	**ours**	**18.78 / 4.447**
90°	1000	MeshGraphNets	44.69 / 11.86
90°	1000	**ours**	**4.105 / 1.841**

Table 2: Physically imbalanced force. We compare the physically imbalanced force in the predictions from MeshGraphNets and our approach for different fiber orientations and force densities. Our approach significantly reduces both the average and the peak error.

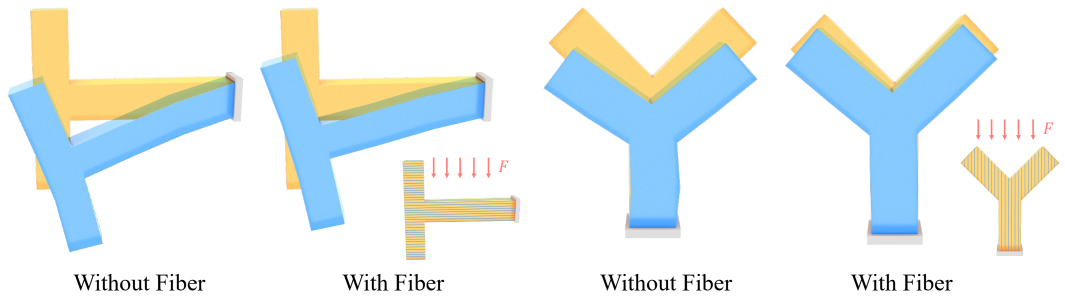

Figure 7: Network generalization. We apply our approach to geometries significantly different from our training set. As can be seen from these two examples, the embedded reinforcement fibers play a crucial role in determining the deformed configurations. This material anisotropy is faithfully captured by our approach. The rest and deformed states are shown in orange and blue respectively.

5 Conclusion

We have presented a novel mesh-based graph neural network architecture for learning the elastodynamics of anisotropic elastic materials. Whereas state-of-the-art approaches are limited to isotropic materials, we propose a novel and easy-to-implement edge feature decomposition scheme that preserves directional information during message passing and thus allows for the modeling of material anisotropies. We demonstrate on a set of qualitative and quantitative examples that our approach outperforms the state-of-the-art method by significant margins. Although we focus on nonlinear elasticity in this work, we believe that our feature decomposition scheme can benefit other applications of graph neural networks that involve direction-dependent behavior.

5.1 Limitation and Future Work

While our approach generalizes well to unseen meshes with similar resolution, we would like to leverage hierarchical representations (51; 50) to apply our approach across a wider range of mesh resolutions. Another interesting avenue for future research is to leverage our neural representation as an efficient and smooth surrogate model for inverse design tasks, *e.g.* shape optimization, where analytical derivatives can be easily obtained through auto differentiation of the network. Finally, our current formulation enables efficient self-supervised learning of anisotropic material properties through physics-based training losses. In the future, we would like to include measurements from real data to obtain neural representations of fiber-reinforced mechanical metamaterials.

REFERENCES

[1] William Fortune Smith. Principles of materials science and engineering. 1986.

[2] Tobias Pfaff, Meire Fortunato, Alvaro Sanchez-Gonzalez, and Peter W. Battaglia. Learning mesh-based simulation with graph networks, 2021.

[3] Artur Grigorev, Bernhard Thomaszewski, Michael J. Black, and Otmar Hilliges. Hood: Hierarchical graphs for generalized modelling of clothing dynamics, 2023.

[4] Robert A Gingold and Joseph J Monaghan. Smoothed particle hydrodynamics: theory and application to non-spherical stars. *Monthly notices of the royal astronomical society*, 181(3):375–389, 1977.

[5] Alexey Shutov and Vladislav Klyuchantsev. On the application of sph to solid mechanics. In *Journal of Physics: Conference Series*, volume 1268, page 012077. IOP Publishing, 2019.

[6] Mathieu Desbrun and Marie-Paule Gascuel. Smoothed particles: A new paradigm for animating highly deformable bodies. In *Computer Animation and Simulation'96: Proceedings of the Eurographics Workshop in Poitiers, France, August 31–September 1, 1996*, pages 61–76. Springer, 1996.

[7] Yongning Zhu and Robert Bridson. Animating sand as a fluid. *ACM Transactions on Graphics (TOG)*, 24(3):965–972, 2005.

[8] Jeremiah U Brackbill, Douglas B Kothe, and Hans M Ruppel. Flip: a low-dissipation, particle-in-cell method for fluid flow. *Computer Physics Communications*, 48(1):25–38, 1988.

[9] Francis H Harlow. The particle-in-cell method for numerical solution of problems in fluid dynamics. Technical report, Los Alamos National Lab.(LANL), Los Alamos, NM (United States), 1962.

[10] Robert W Sumner, James F O'Brien, and Jessica K Hodgins. Animating sand, mud, and snow. In *Computer Graphics Forum*, volume 18, pages 17–26. Wiley Online Library, 1999.

[11] Deborah Sulsky, Shi-Jian Zhou, and Howard L Schreyer. Application of a particle-in-cell method to solid mechanics. *Computer physics communications*, 87(1-2):236–252, 1995.

[12] Chenfanfu Jiang, Craig Schroeder, Andrew Selle, Joseph Teran, and Alexey Stomakhin. The affine particle-in-cell method. *ACM Transactions on Graphics (TOG)*, 34(4):1–10, 2015.

[13] Wing Kam Liu, Shaofan Li, and Harold S Park. Eighty years of the finite element method: Birth, evolution, and future. *Archives of Computational Methods in Engineering*, 29(6):4431–4453, 2022.

[14] Olek C Zienkiewicz, Robert L Taylor, and Jian Z Zhu. *The finite element method: its basis and fundamentals*. Elsevier, 2005.

[15] Ted Belytschko, Wing Kam Liu, Brian Moran, and Khalil Elkhodary. *Nonlinear finite elements for continua and structures*. John wiley & sons, 2014.

[16] Eftychios Sifakis and Jernej Barbic. Fem simulation of 3d deformable solids: a practitioner's guide to theory, discretization and model reduction. In *Acm siggraph 2012 courses*, pages 1–50. 2012.

[17] Sebastian Martin, Bernhard Thomaszewski, Eitan Grinspun, and Markus Gross. Example-based elastic materials. In *ACM SIGGRAPH 2011 papers*, pages 1–8. 2011.

[18] Minchen Li, Zachary Ferguson, Teseo Schneider, Timothy R Langlois, Denis Zorin, Daniele Panozzo, Chenfanfu Jiang, and Danny M Kaufman. Incremental potential contact: intersection-and inversion-free, large-deformation dynamics. *ACM Trans. Graph.*, 39(4):49, 2020.

[19] Theodore Kim and David Eberle. Dynamic deformables: implementation and production practicalities. In *ACM SIGGRAPH 2020 Courses*, pages 1–182. 2020.

[20] Breannan Smith, Fernando De Goes, and Theodore Kim. Stable neo-hookean flesh simulation. *ACM Transactions on Graphics (TOG)*, 37(2):1–15, 2018.

[21] Geoffrey Irving, Joseph Teran, and Ronald Fedkiw. Invertible finite elements for robust simulation of large deformation. In *Proceedings of the 2004 ACM SIGGRAPH/Eurographics symposium on Computer animation*, pages 131–140, 2004.

[22] Hongyi Xu, Yijing Li, Yong Chen, and Jernej Barbič. Interactive material design using model reduction. *ACM Transactions on Graphics (TOG)*, 34(2):1–14, 2015.

[23] Yin Yang, Dingzeyu Li, Weiwei Xu, Yuan Tian, and Changxi Zheng. Expediting precomputation for reduced deformable simulation. *ACM Trans. Graph*, 34(6), 2015.

[24] Theodore Kim and Doug L James. Skipping steps in deformable simulation with online model reduction. In *ACM SIGGRAPH Asia 2009 papers*, pages 1–9. 2009.

[25] Theodore Kim and John Delaney. Subspace fluid re-simulation. *ACM Transactions on Graphics (TOG)*, 32(4):1–9, 2013.

[26] Seunghwan Lee, Ri Yu, Jungnam Park, Mridul Aanjaneya, Eftychios Sifakis, and Jehee Lee. Dexterous manipulation and control with volumetric muscles. *ACM Transactions on Graphics (TOG)*, 37(4):1–13, 2018.

[27] Bohan Wang, Yili Zhao, and Jernej Barbič. Botanical materials based on biomechanics. *ACM Transactions on Graphics (TOG)*, 36(4):1–13, 2017.

[28] Joshuah Wolper, Yunuo Chen, Minchen Li, Yu Fang, Ziyin Qu, Jiecong Lu, Meggie Cheng, and Chenfanfu Jiang. Anisompm: Animating anisotropic damage mechanics: Supplemental document. *ACM Trans. Graph*, 39(4), 2020.

[29] Theodore Kim, Fernando De Goes, and Hayley Iben. Anisotropic elasticity for inversion-safety and element rehabilitation. *ACM Transactions on Graphics (TOG)*, 38(4):1–15, 2019.

[30] Daniel Garcia-Gonzalez, A Jérusalem, Sara Garzon-Hernandez, Ramón Zaera, and A Arias. A continuum mechanics constitutive framework for transverse isotropic soft tissues. *Journal of the Mechanics and Physics of Solids*, 112:209–224, 2018.

[31] Jeffrey A Weiss, Bradley N Maker, and Sanjay Govindjee. Finite element implementation of incompressible, transversely isotropic hyperelasticity. *Computer methods in applied mechanics and engineering*, 135(1-2):107–128, 1996.

[32] Yijing Li and Jernej Barbič. Stable anisotropic materials. *IEEE transactions on visualization and computer graphics*, 21(10):1129–1137, 2015.

[33] Jiong Chen, Hujun Bao, Tianyu Wang, Mathieu Desbrun, and Jin Huang. Numerical coarsening using discontinuous shape functions. *ACM Transactions on Graphics (TOG)*, 37(4):1–12, 2018.

[34] Chenfanfu Jiang, Theodore Gast, and Joseph Teran. Anisotropic elastoplasticity for cloth, knit and hair frictional contact. *ACM Transactions on Graphics (TOG)*, 36(4):1–14, 2017.

[35] Saakaar Bhatnagar, Yaser Afshar, Shaowu Pan, Karthik Duraisamy, and Shailendra Kaushik. Prediction of aerodynamic flow fields using convolutional neural networks. *Computational Mechanics*, 64:525–545, 2019.

[36] Dmitrii Kochkov, Jamie A Smith, Ayya Alieva, Qing Wang, Michael P Brenner, and Stephan Hoyer. Machine learning–accelerated computational fluid dynamics. *Proceedings of the National Academy of Sciences*, 118(21):e2101784118, 2021.

[37] Yue Li, Marc Habermann, Bernhard Thomaszewski, Stelian Coros, Thabo Beeler, and Christian Theobalt. Deep physics-aware inference of cloth deformation for monocular human performance capture. In *2021 International Conference on 3D Vision (3DV)*, pages 373–384. IEEE, 2021.

[38] Kiwon Um, Xiangyu Hu, and Nils Thuerey. Liquid splash modeling with neural networks. In *Computer Graphics Forum*, volume 37, pages 171–182. Wiley Online Library, 2018.

[39] Mianlun Zheng, Yi Zhou, Duygu Ceylan, and Jernej Barbic. A deep emulator for secondary motion of 3d characters. In *Proceedings of the IEEE/CVF Conference on Computer Vision and Pattern Recognition*, pages 5932–5940, 2021.

[40] Mahdad Eghbalian, Mehdi Pouragha, and Richard Wan. A physics-informed deep neural network for surrogate modeling in classical elasto-plasticity. *Computers and Geotechnics*, 159:105472, 2023.

[41] Yue Li, Stelian Coros, and Bernhard Thomaszewski. Neural metamaterial networks for nonlinear material design. *arXiv preprint arXiv:2309.10600*, 2023.

[42] Maziar Raissi, Paris Perdikaris, and George E Karniadakis. Physics-informed neural networks: A deep learning framework for solving forward and inverse problems involving nonlinear partial differential equations. *Journal of Computational physics*, 378:686–707, 2019.

[43] Jonas Zehnder, Yue Li, Stelian Coros, and Bernhard Thomaszewski. Ntopo: Mesh-free topology optimization using implicit neural representations. *Advances in Neural Information Processing Systems*, 34:10368–10381, 2021.

[44] Navami Kairanda, Marc Habermann, Christian Theobalt, and Vladislav Golyanik. Neuralclothsim: Neural deformation fields meet the kirchhoff-love thin shell theory. *arXiv preprint arXiv:2308.12970*, 2023.

[45] Hugo Bertiche, Meysam Madadi, and Sergio Escalera. Neural cloth simulation. *ACM Transactions on Graphics (TOG)*, 41(6):1–14, 2022.

[46] Honglin Chen, Rundi Wu, Eitan Grinspun, Changxi Zheng, and Peter Yichen Chen. Implicit neural spatial representations for time-dependent pdes. In *International Conference on Machine Learning*, pages 5162–5177. PMLR, 2023.

[47] Franco Scarselli, Marco Gori, Ah Chung Tsoi, Markus Hagenbuchner, and Gabriele Monfardini. The graph neural network model. *IEEE transactions on neural networks*, 20(1):61–80, 2008.

[48] Peter W Battaglia, Jessica B Hamrick, Victor Bapst, Alvaro Sanchez-Gonzalez, Vinicius Zambaldi, Mateusz Malinowski, Andrea Tacchetti, David Raposo, Adam Santoro, Ryan Faulkner, et al. Relational inductive biases, deep learning, and graph networks. arxiv 2018. *arXiv preprint arXiv:1806.01261*, 2018.

[49] Zonghan Wu, Shirui Pan, Fengwen Chen, Guodong Long, Chengqi Zhang, and S Yu Philip. A comprehensive survey on graph neural networks. *IEEE transactions on neural networks and learning systems*, 32(1):4–24, 2020.

[50] Meire Fortunato, Tobias Pfaff, Peter Wirnsberger, Alexander Pritzel, and Peter Battaglia. Multiscale meshgraphnets. *arXiv preprint arXiv:2210.00612*, 2022.

[51] Yadi Cao, Menglei Chai, Minchen Li, and Chenfanfu Jiang. Efficient learning of mesh-based physical simulation with bi-stride multi-scale graph neural network. 2023.

[52] Alvaro Sanchez-Gonzalez, Jonathan Godwin, Tobias Pfaff, Rex Ying, Jure Leskovec, and Peter Battaglia. Learning to simulate complex physics with graph networks. In *International conference on machine learning*, pages 8459–8468. PMLR, 2020.

[53] Filipe De Avila Belbute-Peres, Thomas Economon, and Zico Kolter. Combining differentiable pde solvers and graph neural networks for fluid flow prediction. In *international conference on machine learning*, pages 2402–2411. PMLR, 2020.

[54] Kelsey R Allen, Yulia Rubanova, Tatiana Lopez-Guevara, William Whitney, Alvaro Sanchez-Gonzalez, Peter Battaglia, and Tobias Pfaff. Learning rigid dynamics with face interaction graph networks. *arXiv preprint arXiv:2212.03574*, 2022.

[55] Tobias Pfaff, Meire Fortunato, Alvaro Sanchez-Gonzalez, and Peter W Battaglia. Learning mesh-based simulation with graph networks. *arXiv preprint arXiv:2010.03409*, 2020.

[56] Mengyu Chu and Nils Thuerey. Data-driven synthesis of smoke flows with cnn-based feature descriptors. *ACM Transactions on Graphics (TOG)*, 36(4):1–14, 2017.

[57] Jonathan Tompson, Kristofer Schlachter, Pablo Sprechmann, and Ken Perlin. Accelerating eulerian fluid simulation with convolutional networks. In *International Conference on Machine Learning*, pages 3424–3433. PMLR, 2017.

[58] Kaiming He, Xiangyu Zhang, Shaoqing Ren, and Jian Sun. Deep residual learning for image recognition. In *Proceedings of the IEEE conference on computer vision and pattern recognition*, pages 770–778, 2016.

[59] David Baraff and Andrew Witkin. Large steps in cloth simulation. In *Seminal Graphics Papers: Pushing the Boundaries, Volume 2*, pages 767–778. 2023.

[60] Javier Bonet and Richard D Wood. *Nonlinear continuum mechanics for finite element analysis*. Cambridge university press, 1997.

[61] Diederik P Kingma and Jimmy Ba. Adam: A method for stochastic optimization. *arXiv preprint arXiv:1412.6980*, 2014.

[62] Stefan Elfwing, Eiji Uchibe, and Kenji Doya. Sigmoid-weighted linear units for neural network function approximation in reinforcement learning. *Neural networks*, 107:3–11, 2018.